9

The Tropical Ice Core Record of ENSO

LONNIE G. THOMPSON,[1,2] KEITH A. HENDERSON,[1,2] ELLEN MOSLEY-THOMPSON,[1,3] AND PING-NAN LIN[1]

[1]*Byrd Polar Research Center, The Ohio State University, 108 Scott Hall, 1090 Carmack Road, Columbus, Ohio 43210-1002*
[2]*Department of Geological Sciences, The Ohio State University, Columbus, Ohio*
[3]*Department of Geography, The Ohio State University, Columbus, Ohio*

Abstract

Ice core records from tropical and subtropical ice caps provide unique information about the chemical and physical character of the atmosphere. Seasonal variations in the chemical composition of the snowfall and amount of precipitation accumulating on these ice caps produce annual laminations that allow these stratigraphic sequences to be dated. The thickness of an annual lamination reflects the net accumulation, while the physical and chemical constituents (e.g., dust, $\delta^{18}O$, various ions) record atmospheric conditions during deposition. The information presented in this chapter builds upon an earlier investigation of the preservation of an El Niño/Southern Oscillation (ENSO) history in the 1,500-year record from ice cores recovered from the Quelccaya ice cap, Peru (Thompson et al. 1992).

Recent ice cores from Nevado Huascarán, Peru (90°7′S, 77°37′W, 6,048 m), which provided the first tropical ice core history extending back to the Late Glacial Stage (Thompson et al. 1995), also contain an annually resolvable record for the past 270 years. This study is based upon the most recent 68-year period from the Huascarán ice cores, from which a methodology for isolation of ENSO events is developed.

The Quelccaya ENSO study (Thompson et al. 1992) revealed that in the Peruvian Andes the ice core constituent most highly correlated with sea surface temperatures (SSTs) is $\delta^{18}O$ ($r = 0.36$, significant at the 95% level). The current investigation is based upon a 68-year monthly resolved $\delta^{18}O$ time series from the col of Huascarán. $\delta^{18}O$, as preserved on Huascarán, has been shown to reflect large-scale climatological variability over Amazonia and the western tropical Atlantic on timescales of decades to centuries (Thompson et al. 1995). Over the 25-year period (1968–93) of available climatological observations, the interannual variations of $\delta^{18}O$ are closely related to zonal

wind variations over tropical South America at the 500 hPa level. Limited evidence suggests that the spatial distribution of SST anomalies in the western tropical Atlantic influences the 500 hPa circulation, which affects the isotopic fractionation of moisture advected across Amazonia and subsequently the $\delta^{18}O$ of Andean precipitation.

A composite response to ENSO developed by using superposed epoch analysis suggests that often during ENSO warming, the moisture convergence axis over the Atlantic Ocean is diverted northward, resulting in unusually warm and dry conditions over northeast Brazil and ^{18}O enrichment of snowfall on Huascarán. Roughly one year later, as ENSO declines, the Atlantic trade wind circulation strengthens and the associated cooler, moister conditions over the Amazon result in Andean moisture that is more depleted in ^{18}O. The Huascarán results illustrate how the ENSO signal is recorded in Andean snowfall and provide a methodology for application to other annually resolved ice core records. These include recently recovered tropical ice cores (Sajama, Bolivia) and subtropical ice cores (Dasuopu Glacier, Himalayas of China), which are introduced briefly in the final section of the chapter. The Dasuopu record is most promising in its potential to link ENSO histories from the Andes with monsoonal variability over southern Asia.

Introduction

Oceanographers have known for several decades that temporary redistributions of heat energy occur periodically in the surface waters of the tropical Pacific Ocean and that these events are inherently linked with other unusual phenomena in and around the Pacific basin. This system, now referred to as the El Niño/Southern Oscillation (ENSO), includes both an atmospheric component and an oceanic component that are coupled so that variations in one fluid medium are simultaneously reflected in the other (Enfield 1989). The spatial scale of ENSO influence is now recognized as nearly planet-wide (Fig. 9.1), and as a short-term climate forcing mechanism, ENSO is second only to seasonal changes in the distribution of solar irradiance. Geographical shifts in convective activity result in a variety of climatic teleconnections. Those most commonly associated with the warm phase of the ENSO include: a strong Aleutian low; stronger extratropical westerlies and enhanced rainfall (along the subtropical jets); and droughts in northern Brazil, Australia, and Zimbabwe (Bjerknes 1969). Figure 9.1 illustrates the nature of these persistent responses to ENSO in certain regions and includes for future reference the locations of six tropical and subtropical ice core records.

The term "El Niño" was initially used to identify the annual arrival of a southward warm current along coastal Peru, but now it is more commonly applied to the unusual warm events (i.e., when sea surface temperatures [SSTs] in the eastern Pacific increase by more than one standard deviation). Although the cold phase (La Niña) is observed to be the normal condition in the Pacific, unusual strengthening of the eastern subtropical high, enhanced trade wind circulation, and large negative SST anomalies along the Peruvian coast do occasionally occur.

Even though ENSO is primarily a Pacific basin phenomenon (a similar in-phase oscillation is also found in the Indian Ocean), Atlantic SSTs often reflect a lagged response (about 8 months) to the warming/cooling events in the tropical eastern Pacific.

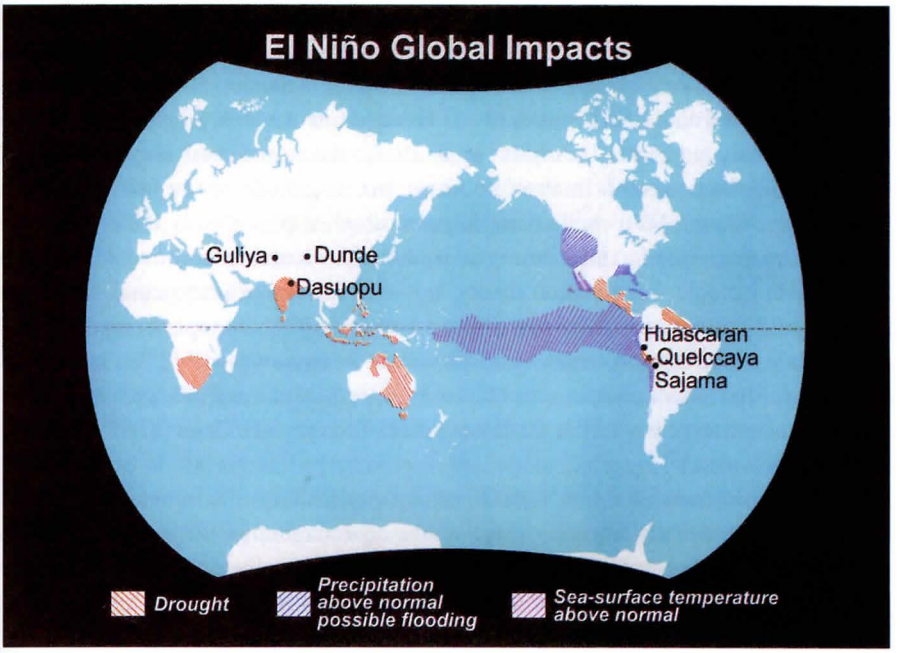

Fig. 9.1 Regional climate changes often experienced during ENSO events are shown along with the locations for tropical and subtropical ice cores discussed in the text. (Modified after NOAA map.)

The mechanism by which Pacific anomalies are transferred (or teleconnected) to the Atlantic basin was described by Covey and Hastenrath (1978). It involves a standing pressure wave between the east tropical Pacific and the west tropical Atlantic such that the nodal pressure boundary that runs generally along the Andean range defines an additional cell component of the east–west Pacific Walker Circulation (Webster 1983). This cell includes the continental surface low positioned between the subtropical anticyclones of the Pacific and Atlantic Oceans as a zone of convergence and rising air, analogous to the large-scale low over the "maritime continents" Australia and Southeast Asia. A series of studies (i.e., Weare 1977; Hastenrath 1978; Lough 1986; Servain and Legler 1986; Servain 1991) using EOF analyses of SST anomalies in the tropical Atlantic clearly showed an analogue to the ENSO variability in the Pacific. The SST anomalies in the tropical Atlantic are substantially weaker than those observed in the equatorial Pacific in association with ENSO (Wallace et al. 1998), but the pattern is quite robust, and there is good evidence based on atmospheric general circulation model simulations (Moura and Shukla 1981; Mechoso et al. 1990) that it is capable of forcing the observed rainfall anomalies. Trenberth et al. 1998 indicate that small changes in SST and SST gradients can lead to shifts in the location of the large-scale organized convection in the tropics and also to changes in the intensity of the convection and hence latent heat release in precipitation and upper tropospheric divergence.

The impact of major ENSO warm events in the tropical Andes is well demonstrated by the 1982–83 and 1997–98 events, which brought major flooding to Ecuador and

northern and central Peru and drought to southern Peru and Bolivia. However, moisture feeding the Andean snowfields is derived almost solely from the east via the trade wind circulation, which implies that the tropical Atlantic is the initial moisture source. Thus, if Pacific SST variability is recorded in Andean precipitation, as the Quelccaya study suggests (Thompson et al. 1984), the signal must first be "filtered" through the Atlantic sector. In absolute terms, the magnitude of the extremes in the ENSO-type Atlantic SST oscillations is much smaller (i.e., 0.8 to 1.2°C) than the Pacific extremes, which exhibit strong coastal Pacific warming of 4 to 5°C. According to basic isotopic fractionation theory, this small range of interannual variability alone should not act as the dominant factor controlling the isotopic composition of atmospheric water vapor or condensate. However, it remains possible that some fluctuations over the Atlantic sector are enhanced via tropical atmospheric processes, such as low-level convergence within the Intertropical Convergence Zone (ITCZ) and over the Amazon basin.

The ability to forecast future ENSO activity, particularly in conjunction with observed twentieth-century warming, relies on the continued improvement of our understanding of the global climate system, as well as on lengthening the temporal perspective of climate variability through the development of high-resolution paleoclimatic records. This study is based upon the annually resolved $\delta^{18}O$ history from two ice cores recovered to bedrock from the center of the Col de Huascarán, whose south summit (6,770 m) marks the highest point in the tropics (**Photo 9.1**). The ice thickness in

Photo 9.1 Huascarán in the Cordillera Blanca of north-central Peru taken at sunset. The drill site is located on the col (6,048 m asl) between the north peak (6,658 m asl) on the left and the south peak (6,768 m above sea level) on the right.

the center of the col is 160–165 m, and it provided a continuous archive of snowfall covering the past 20,000 years (Thompson et al. 1995). Due to the natural thinning of glacier ice, layers corresponding to most of the 20,000 years are found in the bottom 3 m of ice; however, the abundant annual snow accumulation, currently 1.4 to 1.8 m H_2O water equivalent, produces annual layers sufficiently thick that a detailed record of the past 100 years may be reconstructed. With near absolute dating for much of this time period, the Huascarán ice cores constitute a high-resolution proxy record of environmental conditions and thus provide an unprecedented opportunity to explore the ENSO history preserved therein.

It has been demonstrated (Grootes et al. 1989; Rozanski et al. 1997; Thompson and Dansgaard 1975; Thompson et al. 1986) that the relationship between atmospheric temperature and the fractionation of ^{18}O and ^{16}O in moisture deposited in the tropical Andes (as well as on the Dasuopu Glacier on the southern margin of the Plateau of Tibet) is the inverse of that found in higher latitudes where the most ^{18}O-depleted snowfall occurs in the winter. Thus, on Huascarán the seasonal $\delta^{18}O$ cycle exhibits greatest ^{18}O depletion in snowfall arriving during austral summer months. The two primary factors controlling $\delta^{18}O$ here are atmospheric temperature at condensation and the precipitation history of the air mass. Over the annual cycle, precipitation appears dominant via the amount effect, but on longer temporal scales (i.e., decades to centuries), atmospheric temperature is clearly the controlling factor. This is confirmed by the presence of both major and minor large-scale climate events (e.g., Little Ice Age, Younger Dryas, Last Glacial Stage, early Holocene optimum) in Quelccaya (Thompson et al. 1986), Huascarán (Thompson et al. 1995), and Sajama (Thompson et al. 1998).

The characteristic response of $\delta^{18}O$ to ENSO (including both warm and cold events) was explored by using superposed epoch analysis. Each event was centered on the time of the peak SST anomaly along coastal Peru, and then 6-year epochs of monthly averaged $\delta^{18}O$ anomaly and other climatological indices were superposed to form composites from which the mean character of the warm vs. cold events was compared.

Special attention was focused on the most recent 25-year period (1970 to 1994), as additional observations of mid- and upper tropospheric conditions were available over limited areas of South America. These additional data made possible a more in-depth examination of the relationship between $\delta^{18}O$ and temperature, humidity, precipitation, and atmospheric circulation. This is particularly important, as the effect of air temperature on isotopic fractionation in tropical meteoric water reservoirs is opposite to that in the polar regions. Thus, the incorporation of these regional meteorological observations provides an opportunity to identify and better understand the physical mechanisms that translate Pacific events into climatic shifts in the source regions for Andean moisture.

Site Description and Analysis

In July–August 1993, two ice cores to bedrock were recovered from the col between the north and south peaks of Nevado Huascarán, Peru (9°S, 77°30′W, col elevation 6,050 m) (Fig. 9.1, **Photos 9.1 and 9.2**). Ice motion vectors determined from stake

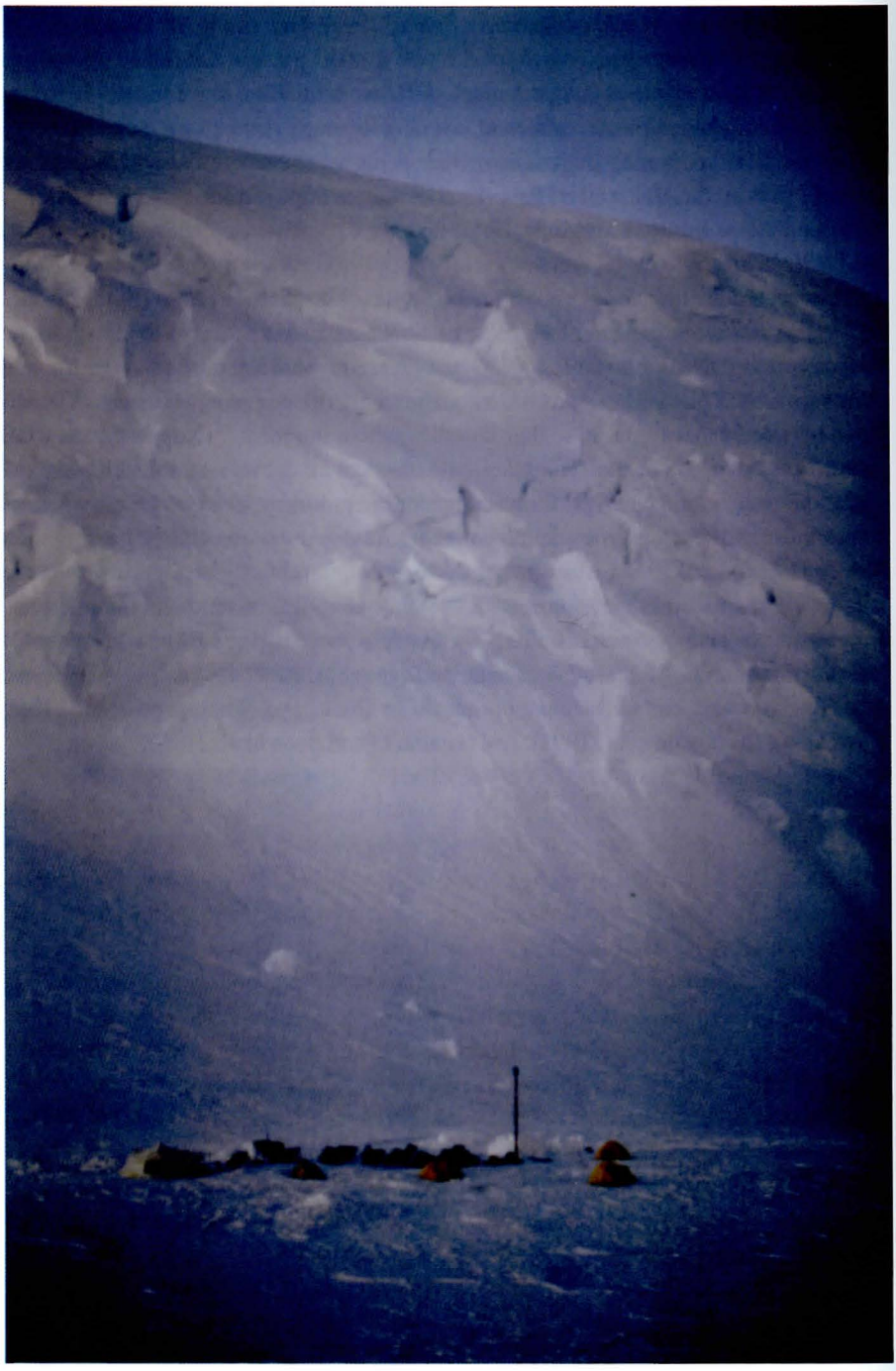

Photo 9.2 The drill camp on the col of Huascarán with the flank of the south peak in the background. The Amazon basin is to the left, and the Pacific Ocean is to the right.

movements from 1991 to 1993 indicate that the drill sites are proximal to the divide between ice flowing toward the east and west outlets of the col. Visible observations and borehole temperatures indicate that the Huascarán is a "polar" type glacier frozen to the bed (Thompson et al. 1995). Core 1, henceforth HSC1, was 160.40 m in length and was cut into 2,677 samples decreasing in thickness from 13 cm at the top to 3 cm at the base. These samples, cut in the field, were melted and poured into 2 or 4 oz. plastic (HDPE) bottles, which were sealed with wax. Core 2, (HSC2), was 166.08 m long and was drilled approximately 100 m from the HSC1 site. Core 2 was returned to the cold room facility at the Byrd Polar Research Center (BPRC) in 1 m long frozen core sections. Roughly six tons of equipment were carried up Huascarán, across crevasse fields (**Photo 9.3**) to the drill site, and over the next 53 days nine tons of equipment, including the two ice cores drilled to bedrock, were carried back down.

Each ice sample from HSC2 was prepared in a Class 100 clean room environment and analyzed for major anion concentrations (Cl^-, NO_3^-, and SO_4^{2-}) by using a Dionex 2010i ion chromatograph. $\delta^{18}O$ was measured by using a Finnigan Mat Delta E mass spectrometer (Craig 1957), and particulate (dust) concentrations and size distributions were determined with a Model TA-II Coulter Counter (Thompson 1973). A second, complete $\delta^{18}O$ profile was also produced from the bottled samples from HSC1, but potential contamination during field preparation precluded dust and anion analyses.

Development of the Time/Depth Relationship

The climate of tropical South America is marked by annual dry seasons (May–October), which are identifiable in the ice cores as elevated concentrations of anion species and dust. The nitrate (NO_3^-) concentrations (Fig. 9.2d) provided the most definitive seasonal marker, but the final timescale was constructed by using a combination of the seasonal oscillations of four ice core constituents as shown in Figure 9.2. Each annual maximum corresponds to the middle of the dry season, assumed to occur on 1 August for the purposes of this analysis. The rapid layer thinning below 120 m limited annual resolution of the record to the most recent 270 years, but the high accumulation and excellent preservation of the seasonal cycles made possible the subannual resolution of $\delta^{18}O$ for 110 annual cycles from 1884 to 1993 (Fig. 9.3).

The accuracy of the ice core timescale is critical for exploration of the relationships among ice core proxy data and tropical climate conditions. The timescale was confirmed to 1980 by comparing the $\delta^{18}O$ record in the 1993 core with that in a 10 m core drilled on Huascarán in 1980 during the original reconnaissance expedition (Thompson et al. 1984). Aside from minor variations in accumulation and modest signal attenuation, the 1993 $\delta^{18}O$ record duplicated the 1980 record for the period of overlap, thus confirming the layer counting back to 1980 as absolute. Three time stratigraphic horizons confirmed the reliability of the layer counting and support precise dating for the uppermost fifty

Photo 9.3 This 16 m ladder crosses a major crevasse on the trail to the col of Huascarán. Roughly six tons of equipment were transported across the crevasse to the col, and nine tons, including two ice cores drilled to bedrock, were carried back down.

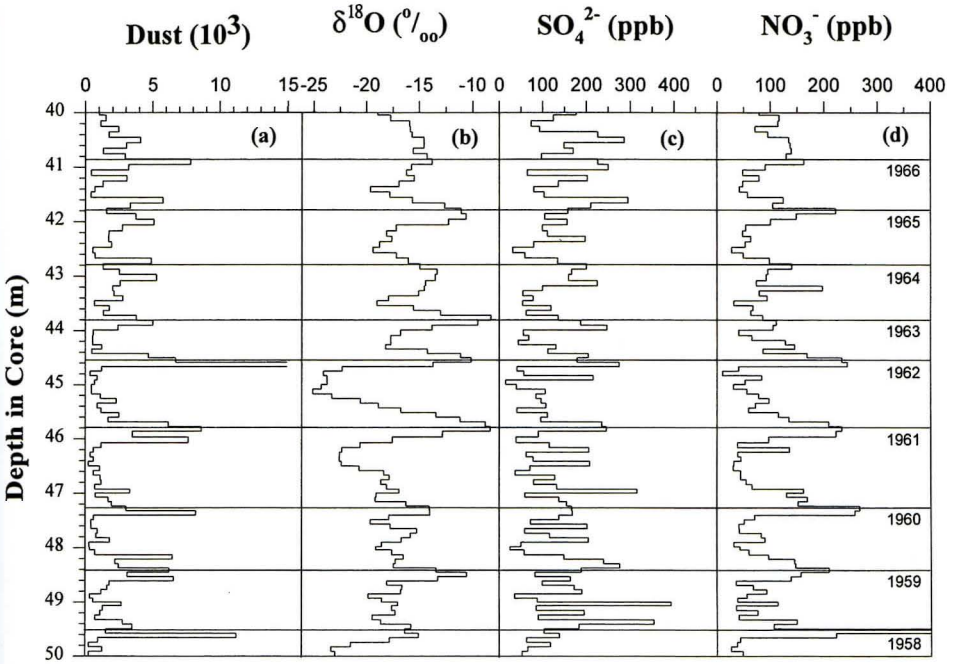

Fig. 9.2 The four seasonally varying constituents used to date the upper part of Huascarán Core 2. These are (a) dust, (b) $\delta^{18}O$, (c) sulfate, and (d) nitrate, shown here for the 40–50 m depth interval. Horizontal lines illustrate the horizons chosen as annual boundaries between successive layers and correspond to snowfall deposited during the middle of the dry season. Dust concentrations are per milliliter sample for particles with diameters of 2.0 m.

years. In May 1970 a magnitude 7.7 earthquake struck coastal Peru, generating large mud flows following the collapse of a large portion of ice from the north peak of Huascarán. The event created a locally fresh sediment source, which is evident in the ice core (Fig. 9.4a) by increased dust deposition for the following four years. Note also that the enhanced dust concentrations during the 1972 and 1973 dry seasons probably reflect the drier conditions associated with that El Niño event. Another time horizon in the HSC2 core is the abrupt increase in ^{36}Cl (Synal et al. 1997). ^{36}Cl is produced by neutron activation during explosion of atomic devices in the presence of a ^{35}Cl source, such as seawater. An abrupt rise in the ^{36}Cl concentration occurs at ~54 m depth (Fig. 9.4b) and is dated to 1952 by layer counting. This spike in ^{36}Cl originated from the 31 October 1952 U.S. "Ivy" surface test of an experimental nuclear device (Carter and Moghissi 1977) on the Eniwetok Atoll in the Pacific Ocean (11°N, 162°E). Finally, in both HSC1 and HSC2, the 1883 eruption of Krakatau, Indonesia (6°S, 105°30′E), produced an anomalous sulfate concentration of ~400 ppb at 110 m depth (Fig. 9.4c), more than twice the concentration of any other sulfate event within a 10 m depth range in the cores. A date of mid-1884 was thus considered to be an absolute time marker for both cores, within the error of the time lag (less than one year).

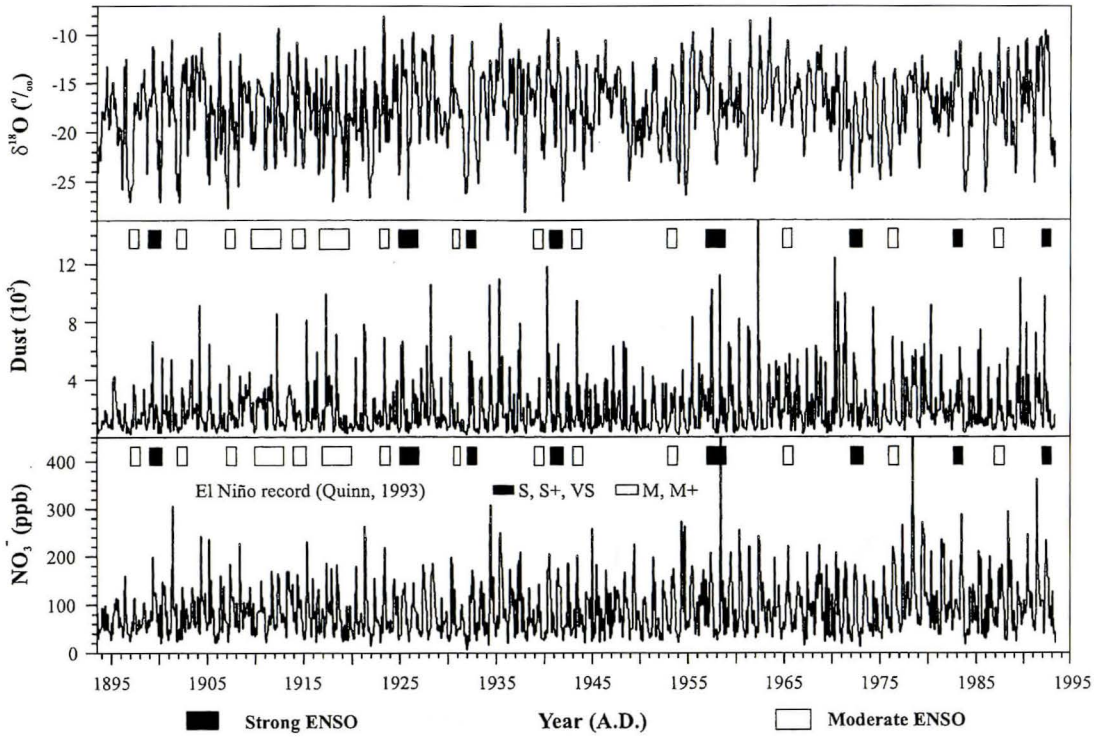

Fig. 9.3 Seasonal variations in the $\delta^{18}O$, insoluble dust, and NO_3^- measured in the Huascarán Core 2 for the past 100 years. Included are the El Niño event identified by Quinn (1993). Note that El Niño strengths are indicated by either solid bars (very strong, strong plus, and strong events) or open bars (moderate and moderate plus events). Weaker El Niño events are not included. Dust concentrations are per milliliter sample for particles with diameters of 2.0 m.

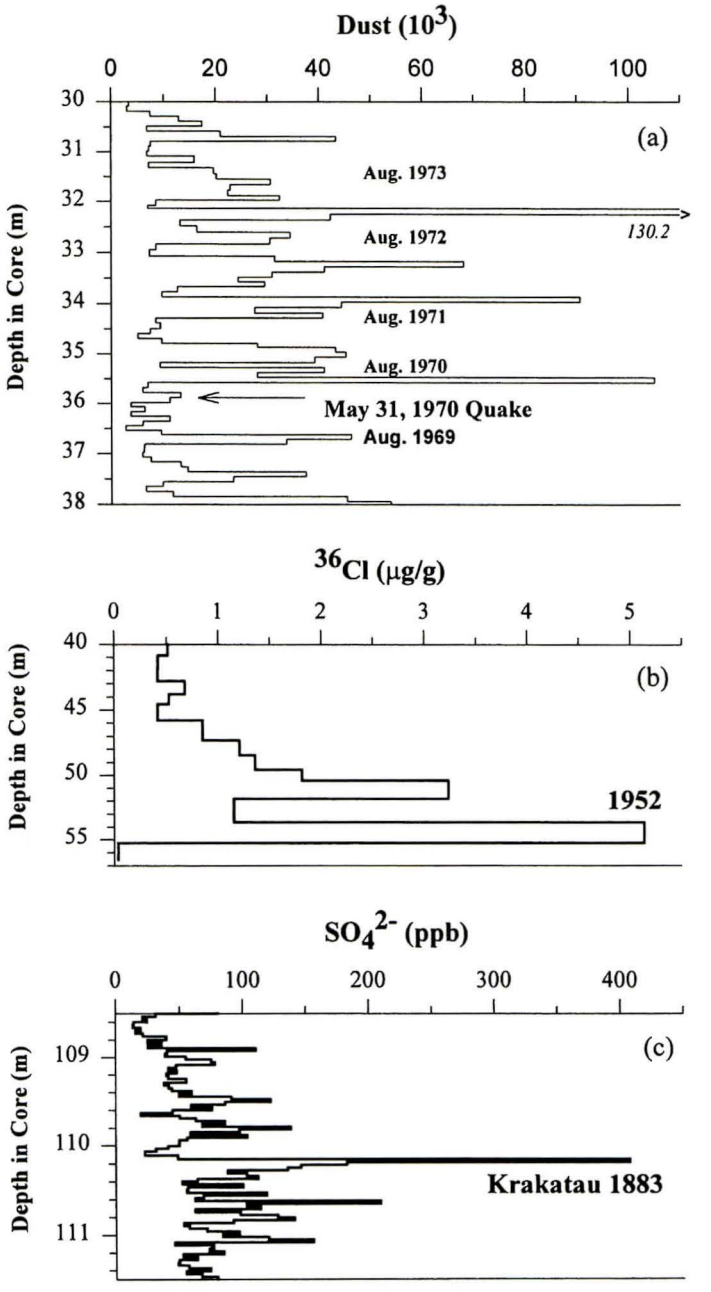

Fig. 9.4 Three different time stratigraphic horizons contribute to the calibration and confirmation of the ice core timescale determined by counting seasonal variations in four different constituents (Fig. 9.2). (a) Dust concentrations were elevated for four years after the 31 May 1970 earthquake in Peru. Dust concentrations are for particles with diameters of 0.63 m per ml sample. (b) The elevated concentration of ^{36}Cl associated with the Ivy test (thermonuclear) on 31 October 1952. (c) Increased sulfate deposition associated with the 1883 eruption of Krakatau.

Construction of Ice Core and Climatological Data Sets for Superposed Epoch Analysis

The high accumulation on Huascarán provided a sample density (number of samples cut per year of accumulation) sufficient to retain monthly resolution for the past 110 years. However, given temporal uncertainties in the earlier portion, only the most recent 68 years were analyzed. To facilitate comparisons among ice core parameters and climatological data sets, the Huascarán $\delta^{18}O$ records were transferred to a timescale with a constant time interval. To construct a continuous "quasi-monthly" time series, the layer thickness representing each "thermal" year (1 August to subsequent 31 July) was divided into 12 units, or bins, of equal thickness or depth. The information for these "artificial" months may deviate from the real months due to variations in annual accumulation rates, differing sample intervals, use of averaging techniques, and poorly defined dry season time markers. Dividing the annual oxygen isotope record into 12 "monthly" increments can be justified since despite the seasonal nature of precipitation in the tropics (measured at lower elevation meteorological stations), the annual oxygen isotopic signal preserved in the ice core is remarkably evenly proportioned between enriched (dry season) and depleted (wet season) isotopic values (Fig. 9.2). The reasons for this are at least twofold. First, although during the dry season it does not rain at lower elevations, often clouds will form at the mountaintops and snow will fall on these high elevation snowfields. Second, it has been known for years from work in the polar regions (i.e., Hammer et al. 1978) that the isotopic input signal from individual snow events is much noisier than the record preserved in the snowpack. The mass exchange by diffusion via the vapor phase in the porous snow usually obliterates the high $\delta^{18}O$ frequencies within a few years, depending on the temperature and the thickness of the individual layers. In areas of high accumulation such as Huascarán, the dominating one year $\delta^{18}O$ cycle remains in the ice. Because on Huascarán this process is largely driven by diurnal heating and cooling, the water vapor is transferred daily up and down the snow column. The net result of this process is an annual signal that represents both dry and wet season isotopic values in the snowpack. Thus, the dry season $\delta^{18}O$ signal is distributed over a greater percentage of each annual increment than might be expected from the annual precipitation patterns observed at the lower altitude meteorological stations.

Within each year, the depth of a sample determined the subannual bin into which its $\delta^{18}O$ value was placed. As many of the years did not contain exactly 12 samples (analyses), adjustments were required. Years containing less than 12 samples (e.g., a sample density (x) < 12) required the insertion of $12 - x$ data points, each calculated as the simple average of the two measurements on either side of the empty bin. In contrast, years with more than 12 samples contained $x - 12$ values calculated as the average of two or more measurements. Only three years were represented by more than 24 samples and thus required averaging three values to create 12 monthly averages. For HSC2, a total of 978 samples encompassed the 823 months (July 1993 to December 1925) considered in this analysis. In summary, 68.8% of the months were represented by an unmodified value, 24.3% represented an average of two values within a "monthly"

bin, 0.5% represented the average of three values within a "monthly" bin, and the remaining 6.4% were created by interpolation.

The identical procedure was performed for the second core, HSC1, and confirmed that this approach captures the temporal fluctuations of $\delta^{18}O$ in Huascarán. For the 820 months (the top 3 months of accumulation were lost in the drilling) covering the top 68 years of HSC1, only 810 samples were cut. The following results were obtained: 72.7% of the months were represented by an unmodified value (a single $\delta^{18}O$ measurement), 12.7% were averages of two samples, 0.1% were averages of three samples, and 14.4% were created by interpolation. Although HSC1 was sampled more coarsely, the major subannual and interannual variations were duplicated (Fig. 9.5a,b) and correlate well, particularly over the past 40 years. Because HSC1 lacks monthly resolution before 1940, HSC2 is considered the better temporally resolved record. Figure 9.6 illustrates the conversion of the HSC2 $\delta^{18}O$ record in the upper 25 m of core (profile a) into the quasi-monthly $\delta^{18}O$ data for 1980–93. The monthly anomalies (Fig. 9.6c) are calculated with respect to their respective long-term climatological means just as monthly anomalies are calculated for meteorological time series.

For the period 1925–93, monthly averaged SST anomalies were created for both the tropical Pacific and Atlantic Oceans. Although SST anomalies are readily available for various regions of the tropical Pacific (e.g., Niño-1, Niño-2, and Niño-3), these indices were not available prior to 1950, and thus they were not used in this analysis. Furthermore, because World War II (WWII) interrupted the commercial and research ship traffic over much of this region, resulting in sparse data collection, data from several sources and various locations were combined to fill any gaps. To complete the coastal Peru record (Pacific SST data set, abbreviated PacSST), the following products were employed:

(1) Coupled Ocean–Atmosphere Data Set (COADS) Monthly Summary Trimmed Groups (MSTG) Group 3 subset (1925–79) – global 2 × 2 grid (Fletcher and Radok 1985);
(2) National Center for Atmospheric Research (NCAR) ds277.0 "recon" SST data set, filtered by empirical orthogonal function (EOF) analysis (1950–92) – COADS grid;
(3) Puerto de Chicama, Peru (74°2′S, 79°27′W) coastal data set (1925–92) (Quispe Arce 1993).

As all three data sets span the period from 1950 through 1979, all anomalies were determined with respect to this common period. Based on the COADS grid, data from five coastal grid boxes (Fig. 9.7), along with the entire Puerto de Chicama time series (continuous through WWII), were used to construct the PacSST data set. Each monthly value was a simple arithmetic mean of all anomaly values (up to six) available. The final construction of the PacSST anomaly time series involved piecing together the COADS and filtered SST series, which were linked by their common climatology (1950–79). For the period from 1950 to 1979 in the final PacSST record, the filtered anomalies series were selected because of the post-treatment. More details are available in Henderson (1996).

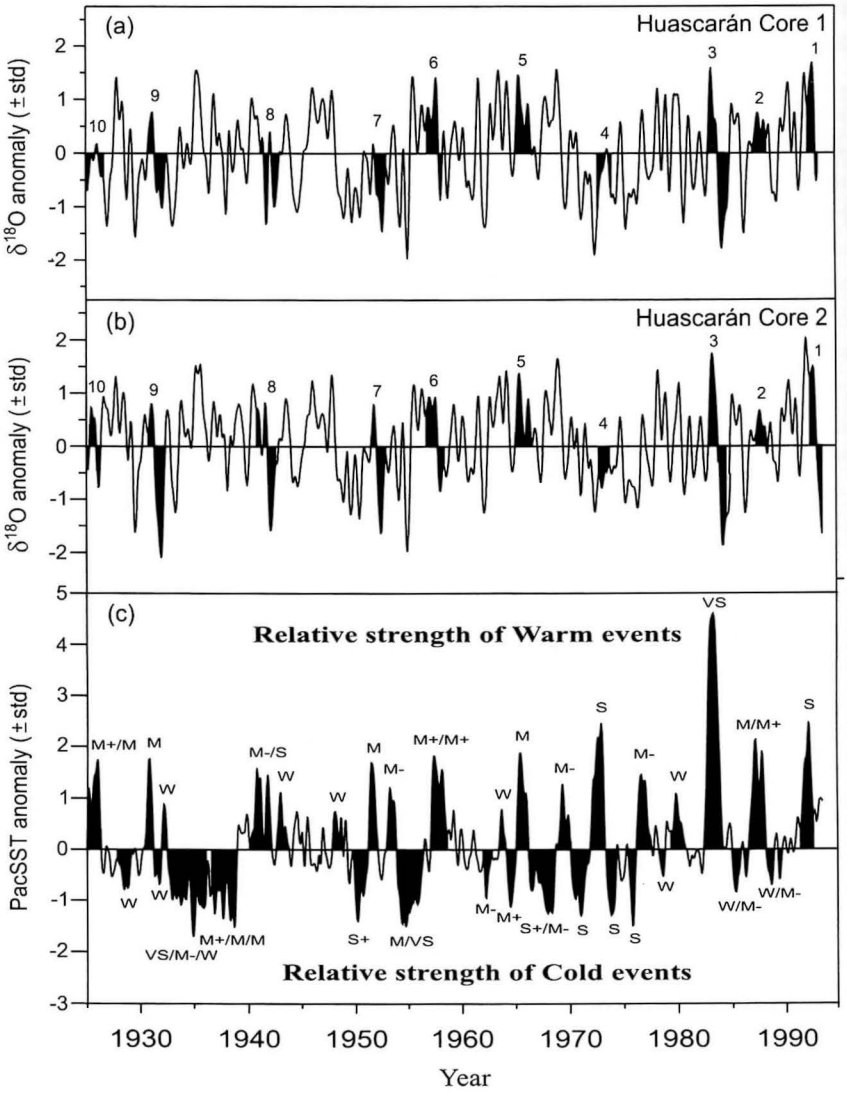

Fig. 9.5 The $\delta^{18}O$ anomaly records from (a) HSC1 and (b) HSC2, both plotted as a seven-sample running mean, with weights determined by a "cosine-bell" function, are compared with (c) the PacSST anomalies for coastal Peru derived from COADS/ds277.0("recon")/Chicama, smoothed by a weighted five-term running mean, for the period 1925–93. Numbered and shaded intervals in (a) and (b) depict the individual $\delta^{18}O$ responses to the ten largest El Niño events (Table 9.1). Letter designations in (c) indicate relative magnitudes of identified El Niño (warm) and La Niña events (see comparison with Quinn, 1993, in Henderson, 1996.)

The centered (adjusted to share a common mean) PacSST anomaly time series (smoothed) for January 1925 through July 1993 is shown in Figure 9.5c. The marked shift to warmer temperatures at about 1940 reflects in part a shift in the COADS data (Folland and Parker 1995) resulting from a sudden change in the use of canvas or

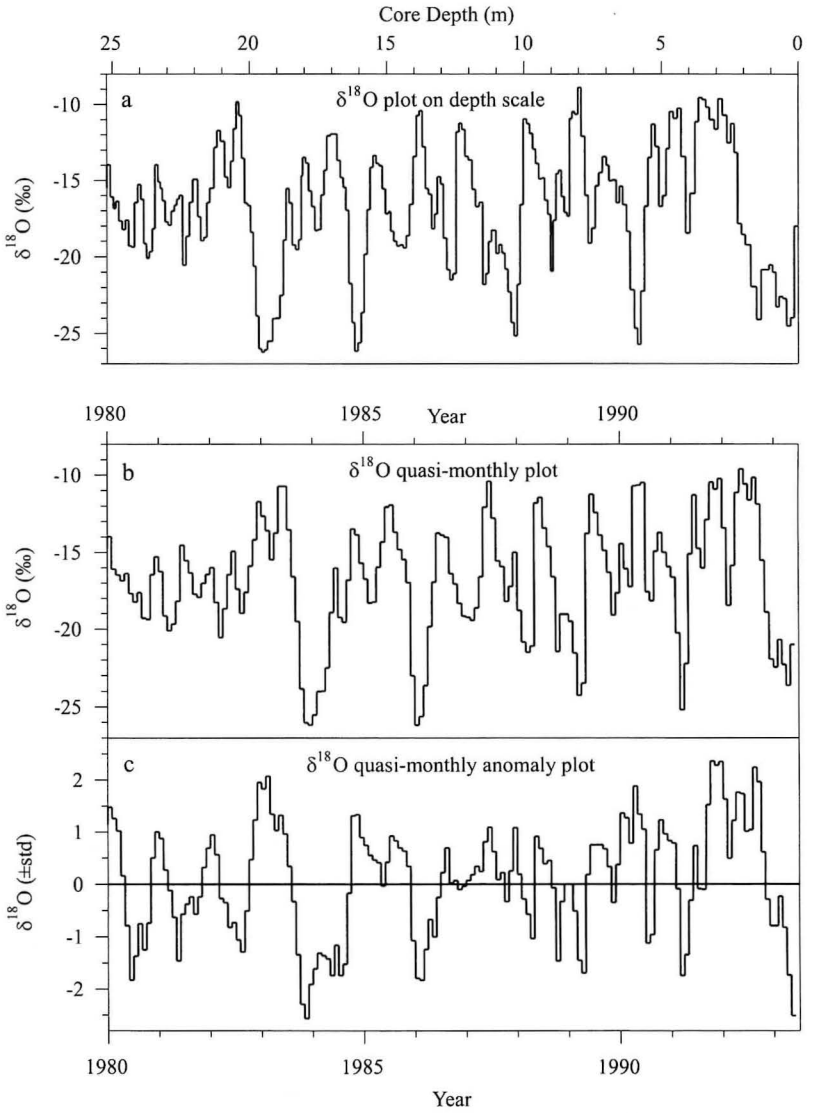

Fig. 9.6 The HSC2 $\delta^{18}O$ record for the upper 25 m of the core shown in (a) was converted to (b) a 13-year $\delta^{18}O$ history with quasi-monthly resolution. The quasi-monthly record was converted to monthly anomalies (c), each calculated with respect to its respective long-term monthly means.

wooden buckets to engine intake thermometers in about 1942. This effect has not been accounted for, as the long-term warming trend is not significant to the problem under investigation here.

The procedures for producing the SST anomaly data sets for portions of the western tropical Atlantic were similar to those for PacSST, and, of course, the Chicama data were not applicable. Because interest in the Atlantic dealt more with the recent record,

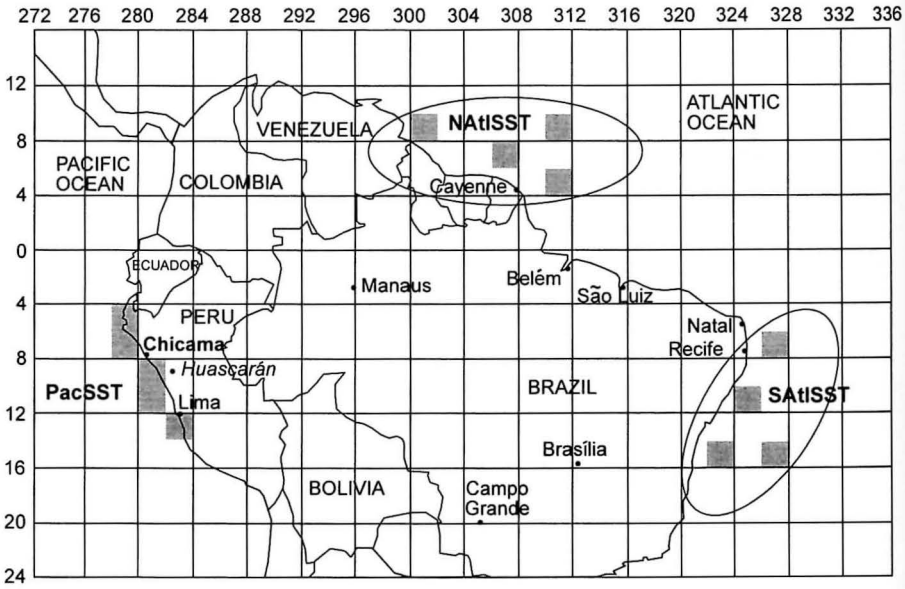

Fig. 9.7 This map shows the location of Nevado Huascarán, the COADS/ds277.0 grid boxes (shaded) used for the creation of PacSST (left), and the meridional Atlantic SST (NAtlSST – SAtlSST) time series (right). The coastal SST monitoring station (Puerto de Chicama) is indicated in boldface. Included are the locations of nine meteorological stations for which surface and upper air data were compiled to create the various tropical South America indices discussed in the text.

only the NCAR ds277.0 "recon" data were used. As the interest in the Atlantic SST data was to explore spatial patterns in the possible source areas for Huascarán moisture, a wider spread of grid points was preferable. Specific grids were selected by their record length and continuity. In earlier work, Henderson (1996) calculated the average SST anomalies for northern, central, and southern coastal regions. The current study employs the average coastal Atlantic SSTs for only two regions (Fig. 9.7): (1) the region off the coast of the Guianas (NAtlSST) and (2) that along the east-central Brazilian coast (SAtlSST). The simple difference between these two anomaly data sets provided a qualitative measure of the meridional heat flux across the moisture source region for Huascarán precipitation.

Monthly averaged surface and upper air data for nine tropical South America locations (Fig. 9.7) were extracted from the journal *Monthly Climatic Data for the World* for 1968 through 1993. Temperature, wind vectors, dew point, and geopotential height data were obtained for three standard levels of the lower and mid-troposphere (850 hPa, 700 hPa, and 500 hPa). Surface data available included temperature, pressure, dew point, and precipitation. For some years data were sporadic, and the individual records were combined into single time series encompassing the entire region surrounding the Amazon basin. Long-term monthly means were determined by using the entire length of the individual records as the basis for the climatology. Anomalies were not standardized in

this case, as the standard deviations were often suspect because of the discontinuities in some of the records.

Superposed Epoch Analysis

The timing, spatial extents, and relative strengths of El Niño events are well known for the past 100 years, although the historical record differs with the choice of the specific indices (both climatological and phenological), which respond differently, some directly and some indirectly, to the ENSO phenomenon. The El Niño record developed by Quinn (1993) extends from A.D. 1525 to the present. His reconstruction was based on sea surface and air temperatures as well as recorded episodic events such as flood damage, mass mortality or migration of sea life, and travel time variations for commercial vessels. As only the physical condition of the ocean should influence the nature of high Andean snowfall, the El Niño record used in this study is based only on the PacSST time series.

The method for classifying events was necessarily subjective, as maximum warming and cooling, the duration of sustained anomalous conditions, and their peak characteristics (e.g., single versus double) were all considered. The letter designations used by Quinn (1993) – VS, S+, S, M+, M, and M– – were retained (Fig. 9.5c), and an additional classification (W) was added for borderline (weak) anomalies. These designations were applied also to cold events (La Niña) in an analogous way. Events displaying two (or three) distinct maxima or minima separated by a significant length of time were classified as 2- or 3-year-events. Although no specific time interval between successive peaks was set, most successive peaks of multiyear events were separated by 10 to 16 months. Unlike Quinn's analysis, each of the multiple peaks was given a separate magnitude rating, and the response of the ice core record was considered for each maximum or minimum.

Eighteen El Niño events (including four 2-year events) total were identified in the PacSST analysis (Table 9.1; Fig. 9.5c), two more than identified by Quinn. Only a few events failed to be identified in each (ice core and SST) record (none of them strong events), with the level of agreement generally improving through time toward the present. Fifteen cold events (six multiyear) total were identified in the PacSST analysis (Fig. 9.5c).

A simple comparison of the PacSST and Huascarán $\delta^{18}O$ anomaly records (Fig. 9.5) reveals little similarity at higher frequencies (1–10 years), with the correlation being virtually zero ($r^2 = 0.0035$). The poor correlation is not due to high-frequency noise, as the correlation of thermal year averages remains negligible ($r^2 = 0.0033$). The possibility of dating errors remains a potential complicating factor, but the absence of any easily visible 4- to 5-year periodicity in the Huascarán $\delta^{18}O$ record indicates the lack of any consistent first-order control by Pacific SSTs. This is not unexpected, as the primary moisture source for Andean snowfall is the Atlantic Ocean and not the Pacific Ocean. This raises the possibility that the $\delta^{18}O$ of Andean snowfall may contain a delayed and modulated response to ENSO via the response of the Atlantic SSTs to Pacific SST (ENSO) forcing.

Table 9.1 *El Niño and La Niña events derived from PacSST anomalies (VS = very strong, S = strong, M = medium, W = weak) for period 1925–1993; each "center month" refers to the mid-point of coastal Pacific (Peru) warming. The ten (nine) El Niño (La Niña) events listed in boldface indicate the subset of events (with M or greater magnitude, one maxima per multiyear event) used to create the $\delta^{18}O$ anomaly composites shown in Figure 9.8c. The individual responses in Huascaran $\delta^{18}O$ to the subset of ten moderate–strong El Niño events are highlighted and numbered sequentially in Figure 9.5.*

El Niño events		La Niña events	
Center month	Strength	Center month	Strength
3/1992	S	5/1989	W
10/1987	M	9/1988	M−
3/1987	M	4/1986	W
2/1983	VS	5/1985	M−
10/1979	W	8/1978	W
8/1976	M−	**11/1975**	S
10/1972	S	**11/1973**	S
5/1969	M−	**1/1971**	S
7/1965	M	**1/1968**	S+
9/1963	W	6/1966	M−
2/1958	M+	**7/1964**	M+
5/1957	M+	3/1962	M−
6/1953	M−	11/1955	M
8/1951	M+	**10/1954**	VS
9/1948	W	**4/1950**	S+
1/1943	W	8/1938	M+
11/1941	M−	10/1937	M
1/1941	S	**12/1936**	M
4/1932	W	**12/1934**	VS
11/1930	M	10/1933	M−
12/1925	M+	12/1932	W
3/1925	M	9/1931	W
		8/1928	W

Based on the conclusion that the Huascarán $\delta^{18}O$ time series does not constitute a direct ENSO paleo-record, the next logical step was to identify and define the characteristic $\delta^{18}O$ response to both warm (El Niño) and cold (La Niña) events and to explore the differences between the two. Bradley et al. (1987) used superposed epoch analysis (SEA) to explore the ENSO signal as preserved in continental temperature and precipitation records of the Northern Hemisphere. The SEA involved the identification of a "zero" point marking the transition from positive to negative Southern Oscillation Index (SOI) (or vice versa) during the onset of an El Niño (La Niña). In each case, April of Year 0 (using the chronology provided by Rasmusson and Carpenter 1982)

was chosen as the "zero" month, as it corresponded to the average occurrence of the SOI sign change. Temperature anomalies were then superposed and averaged for a period beginning 36 months before and ending 36 months after the zero month. Their analysis covered the period from 1881 to 1980 and included twenty-three El Niño (warm) years and twenty La Niña (cold) years. Because the superposition of events by Bradley et al. (1987) assumed an invariant April onset, differences in the timing of the anomaly development were not investigated. In fact, El Niño events develop and peak in different times of the year. For this reason, and as this study includes only a single climate record (so that noise is a concern), the zero month identified for superposition of events was variable. For each event the selected "zero" month was the mid-point of respective coastal Pacific (PacSST) warming. With this exception, the SEA of the PacSST and Huascarán $\delta^{18}O$ anomaly time series followed the procedure described by Bradley et al. (1987).

The 73-month SEA of PacSST and HSC2 $\delta^{18}O$ anomalies for all warm and cold events is shown in Figure 9.8(a and b, respectively). In the 16 months following the peak PacSST anomaly (Fig. 9.8a) evidence appears for an ENSO signature in the Huascarán $\delta^{18}O$ composite (Fig. 9.8b). For El Niño events, $\delta^{18}O$ is enriched for approximately 6–8 months after the zero month after which it changes sign and remains

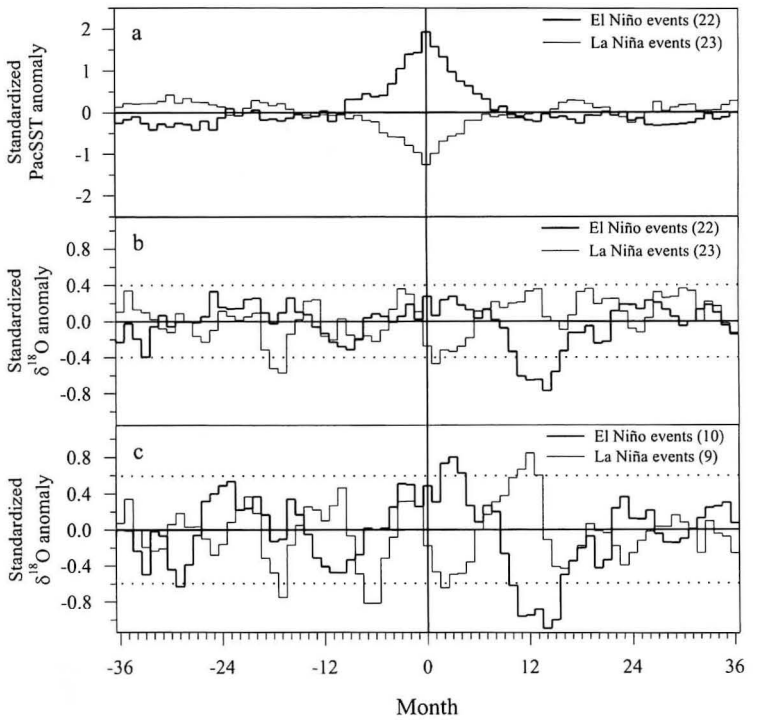

Fig. 9.8 Superposed epoch analysis results (1925–93) for (a) PacSST and (b) Huascarán $\delta^{18}O$ anomalies, both including all identified warm and cold events, and (c) Huascarán $\delta^{18}O$, but only for ENSO events with moderate (M) magnitudes or greater and including only one epoch per each multiyear event. Dotted lines (in b and c) indicate the 95% confidence interval based on 400 Monte Carlo simulations.

depleted for approximately the next 10 months. La Niña events show similar temporal sequences of $\delta^{18}O$ changes, but with opposite sign to those of the warm events. Also evident is an enrichment (depletion) of $\delta^{18}O$ during warm (cold) phases approximately 18–20 months preceding the peak anomaly, which contributes to an apparent (but unsubstantiated) 19-month periodicity. The dotted lines on Figure 9.8 represent the 95% confidence interval based on a Monte Carlo analysis involving 400 simulations of 41 randomly selected and superposed epochs (Bradley et al. 1987).

To further investigate the characteristics of the relationship between ENSO and the $\delta^{18}O$ signal, a second SEA experiment was performed. To accentuate the response to stronger ENSO, (i.e., those most likely to influence Andean precipitation), the weaker events were removed. Also, the secondary maxima (or minima) for multiyear events were eliminated from the composite, except for two cold events for which the second peak was retained, as both were at least two grade levels above those of the initial warm phase. Obviously, the close spacing of maxima or minima (10–16 months) in a 2-year event prohibits back-to-back oscillations (whether high-to-low or low-to-high), as they would overlap and cancel each other. The ten ENSO events of this subset are highlighted in Table 9.1 and numbered sequentially in Figure 9.5 (a, b), and the resulting SEA profiles are shown in Figure 9.8c. The basic characteristics of the responses to warm and cold events remain generally unchanged (comparing Figs. 9.5b and 9.5c); however, in both cases the oscillations are much clearer with the removal of minor events and complicating factors. With the exception of an intriguing 19-month periodicity, the distribution of anomalies in other parts of the 73-month SEA window remains nearly random, indicating that the HSC2 response to PacSST anomalies begin only after the ENSO event has reached peak level.

Relationship between Huascarán $\delta^{18}O$ and Tropical Meteorology

In the previous section, the characteristic ENSO signal in the isotopic composition of archived snowfall in the col of Nevado Huascarán was identified and illustrated. For the purpose of identifying a potential mechanism by which anomalous Pacific SSTs might influence the Andean ice core $\delta^{18}O$ records, it is useful to examine the relationship between the $\delta^{18}O$ interannual variability and conditions of the tropical atmosphere, particularly over the Andean moisture source region. Thus, the time series of the various climatological variables available at the surface and at the 850, 700, and 500 hPa levels were used to explore the relationship between HSC2 $\delta^{18}O$ anomalies and the concomitant tropical climatology. The only statistically significant relationship between $\delta^{18}O$ (Fig. 9.9c) and the meteorological data ($r^2 = 0.30$ for the period 1973–93, averaged quarterly) is with the 500 hPa zonal wind speed anomalies (Fig. 9.9b). Interestingly, the lower-level zonal winds (Fig. 9.9a) display different behavior over this 25-year period and show no clear relationship with either midtropospheric winds (Fig. 9.9b) or the Huascarán $\delta^{18}O$ record (Fig. 9.9c). The lack of any significant relationship between the ice core $\delta^{18}O$ and meteorological conditions (pressure, temperature [Fig. 9.9d], atmospheric layer thickness [Fig. 9.9d], humidity, and rainfall [Fig. 9.9e] anomalies) suggests that "short-term" variations in the $\delta^{18}O$ composition

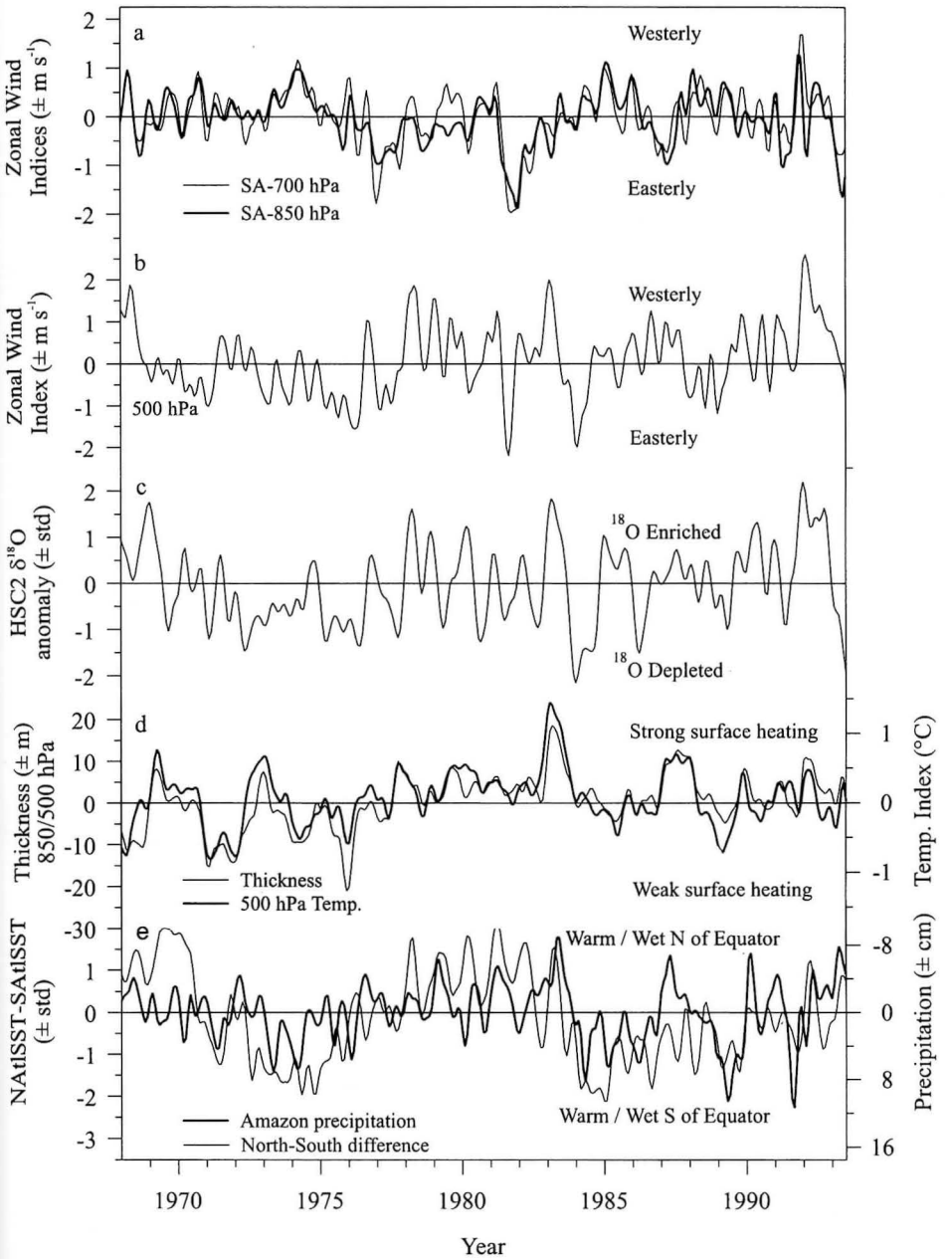

Fig. 9.9 Comparison of (a) zonal wind indices at the 850 and 700 hPa levels, (b) zonal wind index at the 500 hPa level, (c) HSC2 $\delta^{18}O$ anomalies, (d) atmospheric thickness between the 850 and 500 hPa pressure surfaces (light line) and temperature index at the 500 hPa level (dark line), and (e) the NAtlSST−SAtlSST difference in the western tropical Atlantic (light line) and Amazon precipitation anomalies (dark line). For (d) and the rainfall anomalies in (e), only the six northeastern sites (Fig. 9.1) were used. All data were smoothed by a weighted five-term running mean.

of Andean precipitation are not recording regional climate in a recognizable fashion. This is not inconsistent with the earlier observation (see Fig. 9.8) that the relationship between the $\delta^{18}O$ seasonal cycle and atmospheric temperature is reversed in the tropics.

Rayleigh fractionation theory (Jouzel 1986) has been useful in providing a physical link between the water vapor budgets necessary for isotopic depletion and the near-surface atmospheric temperatures over high-latitude ice caps (Dansgaard et al. 1973). While the exact transfer functions have been questioned recently (Cuffey et al. 1995), particularly for different past climate regimes, the temperature – $\delta^{18}O$ relationship in high-latitude environments has been shown empirically to have a consistent (positive) linear relationship (Johnsen et al. 1989). As was noted earlier, for tropical ice fields such as Huascarán, the seasonal $\delta^{18}O$–T relationship is opposite to that in high-latitude areas (i.e., the most depleted values occur in the warmest season). A modeling study by Grootes et al. (1989) invoked Amazon basin hydrology as a controlling mechanism on the Rayleigh "f" parameter ("water vapor fraction remaining") to explain this reverse relationship.

While these attempts at connecting physical mechanisms to the seasonal cycle in tropical meteorology are pertinent to the application of geochemical measurements as climatological proxies, the actual dynamical processes responsible for the interannual isotopic variability (i.e., the $\delta^{18}O$ anomalies) are not sufficiently well established. It is readily apparent that longer (century- to millennial-scale) $\delta^{18}O$ fluctuations in Andean ice cores are primarily temperature dependent as in the higher latitudes. Well-documented recent events such as the Little Ice Age and twentieth-century warming (Thompson et al. 1984) impart strong evidence for this conclusion, but even stronger validation lies in the 6% shift across the glacial–interglacial (Holocene/Wisconsinan) transition and the identification of a Younger-Dryas signature in both the Huascarán (Thompson et al. 1995) and Sajama (Thompson et al. 1998) records. This raises a key question: At what temporal window length does the tropical $\delta^{18}O$–T relationship reverse and become positive?

Although the HSC2 $\delta^{18}O$ record appears to lack direct temporal correlation with zonal wind changes in the lower troposphere, the fairly strong correlation ($r^2 = 0.30$) with the midtropospheric (500 hPa) zonal wind deserves further exploration. Wind velocities at 500 hPa are generally dependent upon the meridional temperature gradient. To approximate the meridional temperature gradient in the source region for Andean moisture, the NAtlSST−SAtlSST difference was calculated (Fig. 9.9e; lighter line). On the multi-annual scale, when SAtlSST is warmer than NAtlSST, the precipitation over the Amazon (south of the equator) is enhanced, leading to enhanced ^{18}O depletion (via the "amount effect") as water vapor traverses the Amazon to the Andes.

Discussion

The characteristic ENSO signal (from the SEA composite) in the Huascarán ice core $\delta^{18}O$ record is represented by a more or less symmetrical wave in the anomaly profiles, with a peak in enrichment (Fig. 9.8c) nearly coincident with the maximum PacSST (Fig. 9.8a) and a peak in ^{18}O depletion about 12 months later. The SEA composites of HSC1 (not shown) are very similar, indicating reproducibility in spite of the lower temporal

resolution of the record. Using the HSC2 SEA $\delta^{18}O$ pattern (Fig. 9.8c) to estimate the influence of individual ENSO events on the Atlantic/Amazon climate regime leads to the conclusion that the influence of the El Niño events of 1992, 1983, 1952, 1941, and 1930 was strong but that ENSO events of 1987, 1972, and 1965 were either weak or had no influence on the Atlantic (Fig. 9.5b).

The lack of a relationship between the composite warm and cold $\delta^{18}O$ signals in the 8 months preceding the SST maximum (i.e., during anomaly growth) indicates that the Huascarán $\delta^{18}O$ ENSO signal is not forced directly by Pacific SSTs. The strong $\delta^{18}O$ response pattern for the 18 months following an ENSO maximum suggests that $\delta^{18}O$ is linked to an ENSO response related to SST in the Atlantic Ocean. This Atlantic sector response must be linked to the Pacific, which accounts for the observed lag. Huascarán remains in a strong trade wind regime throughout the year. However, there is only a moderate response in $\delta^{18}O$ in the year before the zero point, which is dwarfed by the much more significant trailing effect about 12 months later.

The multi-annual scale enrichment of $\delta^{18}O$ in Huascarán precipitation appears prevalent in conjunction with warmer continental temperatures (Fig. 9.9d) and reduced precipitation in Amazonia (Fig. 9.9e). Temperatures at 500 hPa over tropical South America (Fig. 9.9d, dark line) are concomitant with surface temperatures and atmospheric thicknesses (Fig. 9.9d, light line), as the amount of surface heating regulates the height of the tropopause and the height of constant pressure levels (isobaric surfaces). Over the 25-year period investigated (Fig. 9.9), the largest temperature (thickness) changes appear ENSO related, apart from the shift to prolonged warmer conditions occurring from 1975 to 1978. Several of these warm episodes are coincident with enriched $\delta^{18}O$ in HSC2 (particularly in 1983). In the late 1970s the $\delta^{18}O$ record shifts to a more enriched baseline, possibly reflecting the large-scale transition to warmer conditions, which have continued throughout the 1980s.

Many other features of the temperature record are not duplicated in the $\delta^{18}O$ record, suggesting that other regulating factors are at work and need to be identified. For instance, Amazon rainfall appears to have remained above normal for a few years following several of the El Niño events (e.g., 1984 and 1988–89). In the case of 1984, this is reflected in a strong depletion of ^{18}O (a +12-month lagged response), while near-normal temperatures were being recorded over Amazonia.

In comparing the temperature and precipitation anomalies, it is apparent that in many cases, the warm periods (normally during El Niño) are also dry in and around Amazonia, and vice versa (e.g., Kiladis and Diaz 1989). A number of studies have documented the larger scale regional fluctuations during the Pacific ENSO warm and cold phases that involve spatial redistributions of surface temperature anomalies across the entire tropical Atlantic basin (see Anderson et al. 1998). One early such study was that of Hastenrath (1978) who showed that a typical pattern of tropical Atlantic SST anomalies exists (warm off the coast of Angola, and cold near the Caribbean) during times when the low-level convergence axis (ITCZ) is positioned anomalously far south (a condition often coincident with the cold phase of ENSO). This phenomenon has been identified as a cause of high rainfall in the Ceará region of Brazil, the antithesis being the major droughts (secas) that occur there coincident with the stronger Pacific warm events. In Figure 9.9e, this is illustrated by the generally positive relationship between rainfall

anomalies and the NAtlSST–SATlSST difference anomalies. As anecdotal evidence, the abrupt warming of 1975–78 (mentioned earlier) is larger in the Caribbean sector than along the south tropical margin of Brazil (note the positive NAtlSST–SATlSST difference anomalies) and is coincident with a reduction in precipitation over coastal and inland Amazon sites. In 1984 this relationship reversed, with warmer temperatures along the south tropical margin of Brazil coincident with increased rainfall over the Amazon and increased ^{18}O depletion in Huascarán precipitation (Fig. 9.9c).

Further examination of the data suggests that a direct link between the behavior of the zonal winds and SST distribution. Hastenrath (1984) demonstrated that a southward shift of the ITCZ enhances the zonal surface trade winds at 10°S. The expected implication for Andean precipitation is enhanced precipitation and ^{18}O depletion in Amazonian water vapor (0°–10°S) via the "amount effect" when the NAtlSST–SAtlSST index is negative, and vice versa. Support for the trade wind concept also comes from an analysis by Rao et al. (1993), who showed that the strength of the surface wind vector oriented perpendicular to the coast (i.e., southeasterly) determines the amount of rainfall received along the Atlantic margin of Brazil between 5° and 15°S. The suggestion of (unidirectional) velocity convergence as a mechanism controlling rainfall along the water vapor transport path to Huascarán could help to explain the apparent strong linkage between zonal wind strength and ^{18}O depletion in Andean snowfall (Fig. 9.10a). However, this localized "land breeze," coupled with minor topography in eastern Brazil, must be integrated with the hydrologic processes of the remainder of the Amazon basin before any further generalizations are possible. Finally, a recent study of meteorological conditions over the Bolivian altiplano (P. Aceituno, unpublished data) noted that a "plume" of water vapor exists within the midtroposphere over that region. It is worth noting that Newell and Zhu (1994) report the existence of "tropospheric rivers of water vapor" from their analysis of atmospheric specific humidity and wind velocity data. If such a layered structure in atmospheric water vapor were a common phenomenon over large areas of the Andean front, a more quantitative relationship might be derived among the upper air circulation, barrier-generated velocity convergence, and high Andean precipitation.

Future ENSO Research in Light of New Tropical Ice Core Records

The 68-year time series of $\delta^{18}O$ from the Huascarán ice cores is a well-preserved, subannually resolved archive of the environmental conditions over Amazonia and the tropical Atlantic. However, the interannual variations reflect a modified signal of either oceanic or atmospheric temperatures that appear closely related only to zonal wind variations over tropical South America at the 500 hPa level (Fig. 9.9a). There is some evidence that the spatial distribution of sea surface temperature anomalies in the western tropical Atlantic affects the 500 hPa circulation, which in turn influences precipitation over the Amazon basin and ^{18}O fractionation. Also, it is apparent that enrichment (depletion) of ^{18}O in Andean snow is related to a combination of warmer (cooler) atmospheric temperatures and less (more) pluvial conditions. On longer timescales, the control of temperature on $\delta^{18}O$ ratios begins to dominate the effect of precipitation (the amount effect).

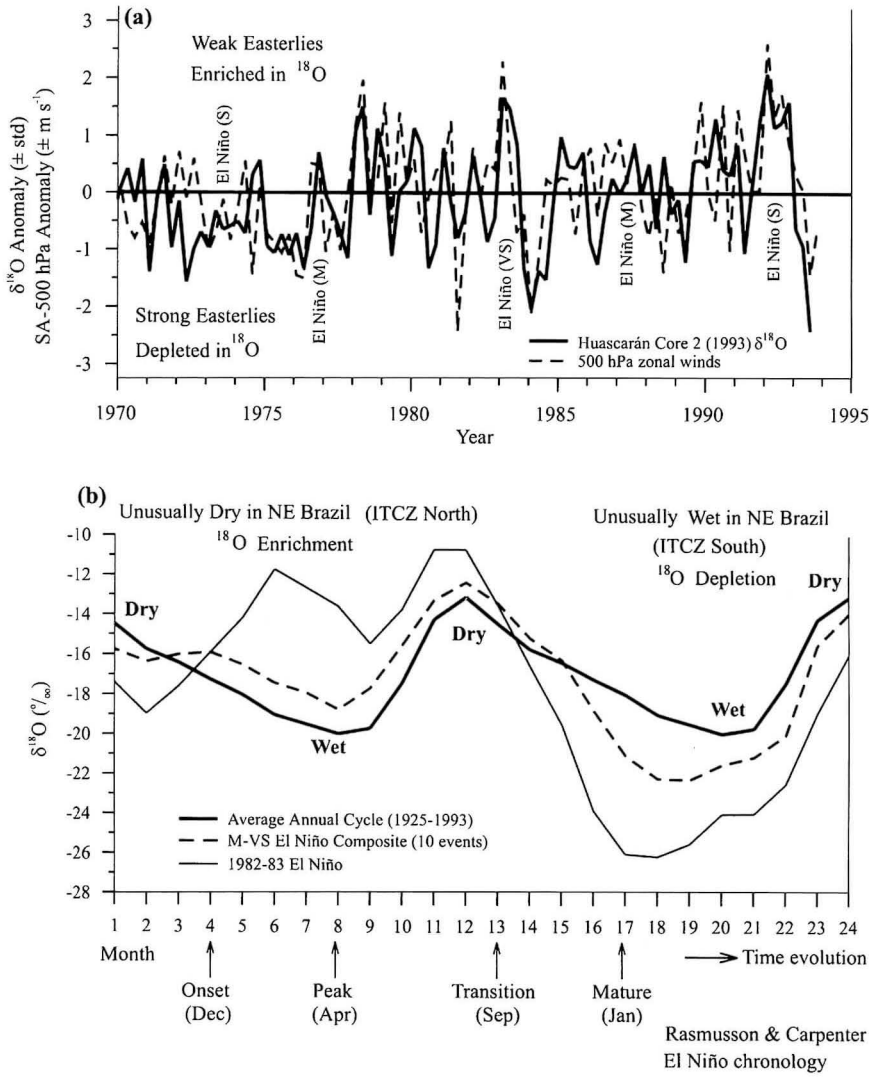

Fig. 9.10 (a) Comparison of $\delta^{18}O$ anomalies (standardized departures from long-term monthly means) from Huascarán Core 2 and a composite index of zonal wind departures at the 500 hPa level derived from radiosonde measurements over nine stations in Brazil and Peru (averaged quarterly from 1970 to 1994). (b) The composite $\delta^{18}O$ response to El Niño events is compared with the $\delta^{18}O$ response of the 1982–83 event and the normal annual variation in $\delta^{18}O$ due to the wet–dry seasonality over the Amazon.

The event-based SEA analysis, involving the superposition of individual warm (El Niño) and cold (La Niña) events, depicts the typical reaction of the Atlantic-driven tropical engine over Amazonia and identifies a characteristic 10- to 14-month half-period $\delta^{18}O$ wave in the composites (Fig. 9.10b). During El Niño, the onset of the disturbance occurs precisely at the peak positive anomaly in Pacific SST, identifiable by the development of strong enrichment of ^{18}O (significant at the 5% level) soon afterward and then a full reversal to strongly ^{18}O-depleted snowfall 10–14 months afterward.

This scenario is illustrated by the schematic in Figure 9.10b, which includes the composite ice core $\delta^{18}O$ records for the ten strong to moderate ENSO events (Fig. 9.8c, dark line), the $\delta^{18}O$ record for the 1982–83 ENSO event (Fig. 9.10b, light solid line), and average annual $\delta^{18}O$ cycle (1925–93). The characteristics of the cold event composites are very similar but opposite, resulting in a strong negative relationship between warm and cold event composites in the year following peak anomaly development (Fig. 9.8c).

In the last year, new ice cores were recovered from two tropical sites: Sajama, Bolivia (18°06′S, 68°53′W; 6,542 m; Fig. 9.1) and Dasuopu Glacier in the Himalayas of China. The records from these cores will complement earlier records from the Quelccaya ice cap (Thompson et al. 1992) and Huascarán (Thompson et al. 1995; Henderson et al. 1999) by increasing the spatial coverage of ice core records in the tropics. Figure 9.11 illustrates the seasonal variations in $\delta^{18}O$, insoluble dust, and NO_3^- concentrations in

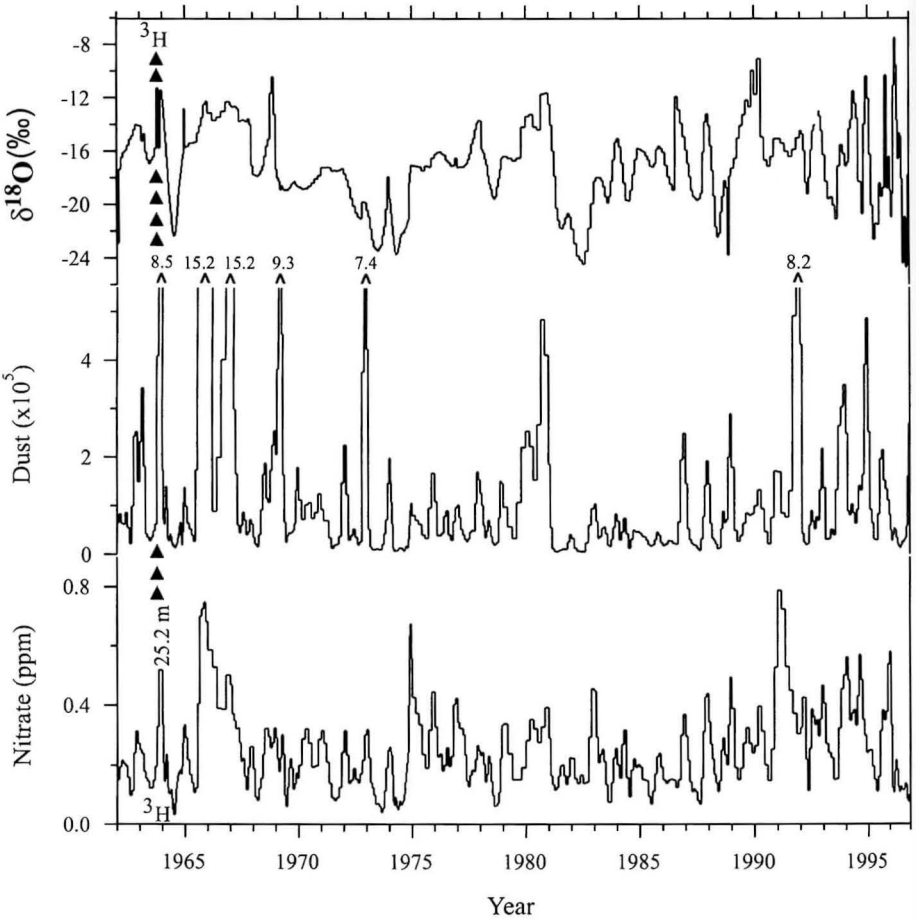

Fig. 9.11 Seasonal variations in $\delta^{18}O$, insoluble dust, and NO_3^- concentrations preserved in the Sajama, Bolivia, ice cores allow dating by layer counting in the upper 50 m of core. Dating is confirmed at 1964 by identification of the 1964 tritium (^3H) peak. The sample values in each plot are smoothed by using a three-point weighted (1,2,1) running mean. Dust concentrations are for particles with diameters of 0.63 m per ml sample.

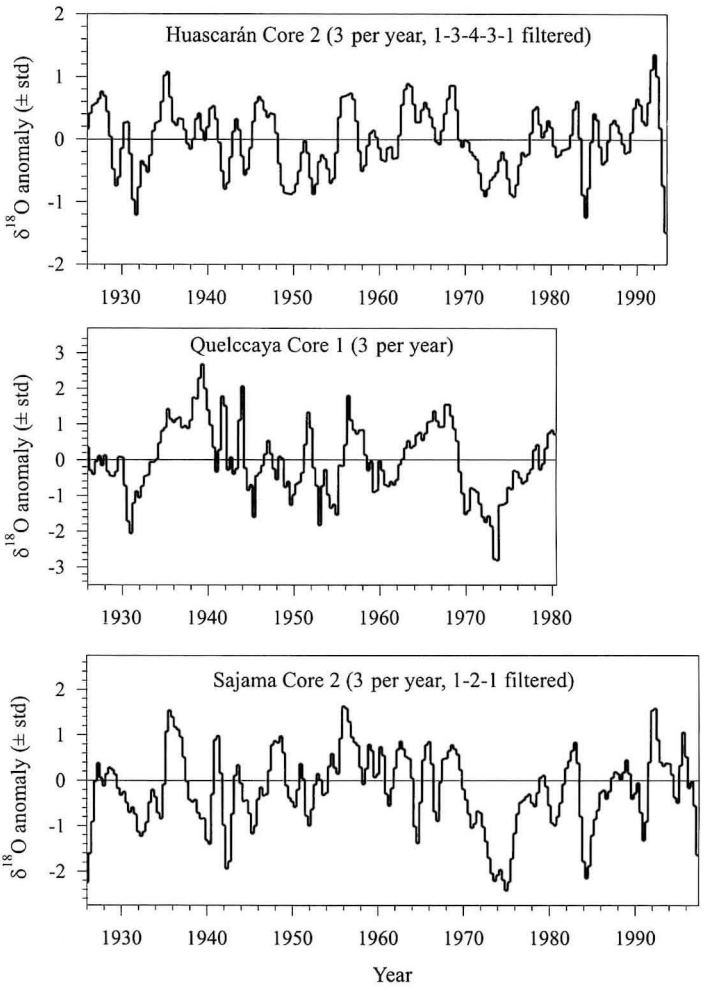

Fig. 9.12 Comparison of $\delta^{18}O$ anomalies along a north to south transect in the tropical Andes: (a) Huascarán, (b) Quelccaya, and (c) Sajama. These plots illustrate both local and regional variability among these sites ranging along the altiplano between 9°S and 18°S.

one of the Sajama cores, which will allow annual layer counting (precise dating) in the upper 50 m. The dating shown has been calibrated by identification of the 1964 tritium (^3H) peak. The sample values in each plot are smoothed by using a three-point (1,2,1) filter (Thompson et al. 1998). The annual resolution in the Sajama records will facilitate detailed comparison with records from Huascarán at 9°S and Quelccaya at 14°S. For example, the $\delta^{18}O$ anomalies from 1928 up to the time the ice cores were recovered (Fig. 9.12) illustrate their similarities and differences north to south in the Andes. Intervals from 1970 to 1978 and from 1930 to 1932 stand out as cold periods (^{18}O depleted) at all three sites. Similarly, warm periods from 1932 to 1970 and 1978 to the present (^{18}O enriched) are also evident at each site. As was discussed previously, in the

Huascarán core the 1982–83 El Niño is characterized by increased seasonal extremes in $\delta^{18}O$ anomalies, a feature also evident in the recently collected Sajama ice core $\delta^{18}O$ record.

There is increasing interest in the nature of the connection between ENSO and monsoonal variability and in particular in how these are linked to rice production in countries such as India (Webster et al. 1998). Several linkages between monsoonal intensity and Tibetan snow cover have been discovered (e.g., Barnett et al. 1989; Yasunari et al. 1991; Vernekar et al. 1995). The changing albedo effect due to snow-cover variations on the high Plateau of Tibet may affect the strength of the Asian monsoon (Sirocko et al. 1993). Barnett et al. (1989) suggested that monsoonal intensity may be affected by the extent and duration of Tibetan snow cover. More snow cover or snow cover extending later into the summer season reduces the sensible heat available to heat the Tibetan plateau surface, potentially resulting in a less intense summer low-pressure system and thus reduced monsoon intensity. This in turn may also affect intensities of ENSO events. On longer timescales, general circulation model simulations indicate that increases in snow and ice cover on the Tibetan plateau during the last glacial maximum, resulting in increases in albedo, may have also caused weakening of the monsoonal circulation (Kutzbach et al. 1998).

Recent ice core records from the Tibetan plateau (Dunde Ice Cap [Thompson et al. 1989] and Guliya Ice Cap [Thompson et al. 1997]) may allow these relationships to be examined on annual to millennial timescales. A new record is being reconstructed from ice cores recovered in 1997 from the Dasuopu Glacier (28°23′N, 85°43′E; 7,200 m asl). Dasuopu, located in an area likely to be influenced by ENSO events (Fig. 9.1), is of particular interest, as it offers an excellent opportunity to compare interannual climate variability in the Himalayas with that in the South American tropical ice cores. In the Himalayas and indeed across most of the Tibetan plateau, 80–90% of the precipitation comes in the wet season (monsoon season) from May to October, which produces distinct annual layers in all relevant ice core constituents. The annual records of $\delta^{18}O$, insoluble dust, and nitrates are shown in Figure 9.13 for the upper part (1973 to 1997) of the Dasuopu core. The black squares indicate major ENSO events, while the open squares indicate moderate or minor ones, over this period. Of particular interest is that the summer monsoon isotopic depletions during many of the ENSO years are not as low as during "normal" years over this period. These relationships will be explored after the analyses of the three new Dasuopu ice cores (149.2 m, 159.6 m, 167.6 m) are completed. Initial results suggest that the record will extend back into the Last Glacial Stage.

Acknowledgments We wish to thank Mary E. Davis, Paul Kinder, Bruce Koci, Vladimir Mikhalenko, Cesar Portocarrero, Willie Tamayo Alegre, Selio Villón, and the team of mountain guides, porters, cooks, and arrieros whose assistance in the field logistics was essential. We also thank Chung-Chieh Wang of The Ohio State University Department of Geography for assistance in computer programming and Steve Worley of NCAR for access to the COADS data. We also gratefully acknowledge Juerg Beer of the Swiss Federal Institute of Environmental Science and Technology, who performed the accelerator mass spectrometry measurements of ^{36}Cl on the ice core.

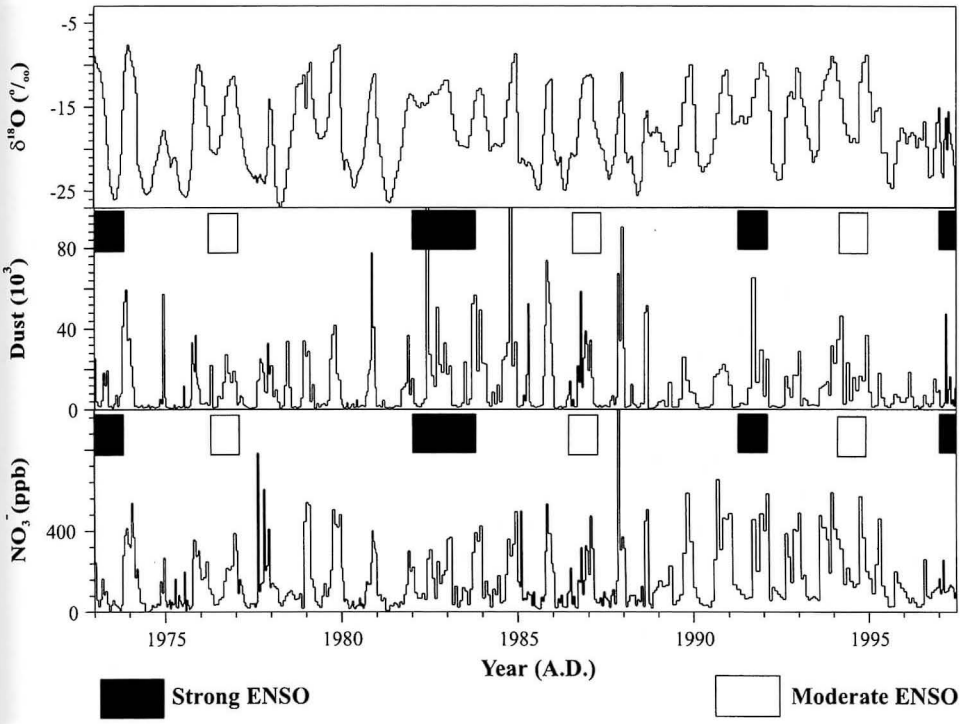

Fig. 9.13 Seasonal variations in $\delta^{18}O$, insoluble dust, and NO_3^- concentrations preserved within Core 1 from the Dasuopu Glacier (Himalayas) allow dating by annual layer counting in the upper 150 m. Dust concentrations are for particles with diameters of 0.63 m per ml sample.

This research was supported under National Oceanic and Atmospheric Administration (NOAA) awards (NA16RC0525 and NA76GP0025). Special thanks to David Goodrich and Mark Eakin of the NOAA Office of Global Programs for their extraordinary efforts to support ice core research in the Andes. This is Contribution Number 1125 of the Byrd Polar Research Center, The Ohio State University.

References

ANDERSON, D. L. T., SARACHIK, E. S., WEBSTER, P. J., and ROTHSTEIN, L. M. (eds.), 1998: *The TOGA Decade, Reviewing the Progress of El Niño Research and Prediction. Journal of Geophysical Research*, **103**, 14,167–14,510.

BARNETT, T., DÜMENIL, L., SCHLESE, U., ROECKNER, E., and LATIF, M., 1989: The effect of Eurasian snow cover on regional and global climate variations. *Journal of the Atmospheric Sciences*, **46**, 661–685.

BJERKNES, J., 1969: Atmospheric teleconnections from the equatorial Pacific. *Monthly Weather Review*, **97**, 163–172.

BRADLEY, R. S., DIAZ, H. F., KILADIS, G. N., and EISCHEID, J. K., 1987: ENSO signal in continental temperature and precipitation records. *Nature*, **327**, 497–501.

CARTER, M. W. and MOGHISSI, A. A., 1977: Three decades of nuclear testing. *Health Physics*, **33**, 55–71.

COVEY, D. L. and HASTENRATH, S., 1978: The Pacific El Niño phenomenon and the Atlantic circulation. *Monthly Weather Review*, **106**, 1280–1287.

CRAIG, H., 1957: Isotopic standards for carbon and oxygen and correction factors for mass spectrometric analysis of carbon dioxide. *Geochimica et Cosmochimica Acta*, **12**, 133–149.

CUFFEY, K. M., CLOW, G. D., ALLEY, R. B., STUVIER, M., WADDINGTON, E. D., and SALTUS, R. W., 1995: Large Arctic temperature change at the Wisconsin-Holocene glacial transition. *Science*, **270**, 455–458.

DANSGAARD, W., JOHNSEN, S., CLAUSEN, H. B., and GUNDESTRUP, N., 1973: Stable isotope glaciology. *Meddelelser Om Grønland*, **192**, 1–53.

ENFIELD, D. B., 1989: El Niño, past and present. *Reviews of Geophysics*, **27**, 159–187.

FLETCHER, J. and RADOK, U., 1985: COADS (Comprehensive Ocean-Atmosphere Data Set) Release 1 Handbook, a joint program by CIRES, NOAA-ERL, NCAR, and NCDC, Boulder, Colorado, 39 pp. plus supplements.

FOLLAND, C. K. and PARKER, D. E., 1995: Correction of instrumental biases in historical sea surface temperature data. *Quarterly Journal of the Royal Meteorological Society*, **121**, 319–367.

GROOTES, P. M., STUIVER, M., THOMPSON, L. G., and MOSLEY-THOMPSON, E., 1989: Oxygen isotope changes in tropical ice, Quelccaya, Peru. *Journal of Geophysical Research*, **94**, 1187–1194.

HAMMER, C. U., CLAUSEN, H. B, DANSGAARD, W., GUNDESTRUP, N., JOHNSEN, S. J., and REEH, N., 1978: Dating of Greenland ice cores by flow models, isotopes, volcanic debris and continental dust. *Journal of Glaciology*, **20**, 3–26.

HASTENRATH, S., 1978: On modes of tropical circulation and climate anomalies. *Journal of the Atmospheric Sciences*, **35**, 2222–2223.

HASTENRATH, S., 1984: Interannual variability and annual cycle: Mechanisms of circulation and climate in the tropical Atlantic sector. *Monthly Weather Review*, **112**, 1097–1107.

HENDERSON, K. A., 1996: *The El Niño–Southern Oscillation and other modes of interannual tropical climate variability as recorded in ice cores from the Nevado Huascarán Col, Peru.* M.S. Thesis, Dept. of Geological Sciences, The Ohio State University, Columbus, Ohio, 194 pp.

HENDERSON, K. A., THOMPSON, L. G., and LIN, P.-N., 1999. Recording of El Niño in ice core $\delta^{18}O$ records from Nevado Huascarán, Peru. *Journal of Geophysical Research* (in press).

JOHNSEN, S. J., DANSGAARD, W., and WHITE, J. C., 1989: The origin of Arctic precipitation under present and glacial conditions. *Tellus*, **41B**, 452–468.

JOUZEL, J., 1986: Isotopes in cloud physics: Multiphase and multistage condensation processes. *In* Fritz, P. and Fontes, J. Ch. (eds.), *Handbook of Environmental Isotope Geochemistry*, Vol. 2 (*The Terrestrial Environment B*). Amsterdam: Elsevier Press, 61–112.

KILADIS, G. N. and DIAZ, H. F., 1989: Global climatic anomalies associated with extremes in the Southern Oscillation, J. *Climate*, **2**, 1069–1090.

KUTZBACH, J., GALLIMORE, R., HARRISON, S., BEHLING, P., SELIN, R., and LAARIF, F., 1998: Climate and biome simulations for the past 21,000 years. *Quaternary Science Reviews*, **17**, 473–506.

LOUGH, J. M., 1986: Tropical Atlantic sea surface temperatures and rainfall variations in Subsaharan Africa, *Monthly Weather Review*, **114**, 561–570.

MECHOSO, C. R., LYONS, S. W., and SPAHR, J. A., 1990: The impact of sea surface temperature anomalies on the rainfall over northeast Brazil. *Journal of Climate*, **3**, 812–826.

MOURA, A. D. and SHUKLA, J., 1981: On the dynamics of droughts in northeast Brazil: Observations, theory and numerical experiments with a general circulation model. *Journal of Atmospheric Sciences*, **38**, 2653–2675.

NEWELL, R. E. and ZHU, Y., 1994: Tropospheric rivers: A one-year record and possible application to ice core data. *Geophysical Research Letters*, **21**, 113–116.

QUINN, W. H., 1993: The large-scale ENSO event, the El Niño and other important regional patterns. *Bulletin de l'Institut Français d'Études Andines*, **22**, 13–34.

QUISPE ARCE, J., 1993: Variaciones de la temperatura superficial del mar en Puerto Chicama y del Índice de Oscilación del Sur: 1925–1992, *Bulletin de l'Institut Français d'Études Andines*, **22**, 111–124.

RAO, V. B., de LIMA, M. C., and FRANCHITO, S. H., 1993: Seasonal and interannual variations of rainfall over eastern northeast Brazil. *Journal of Climate*, **6**, 1754–1763.

RASMUSSON, E. M. and CARPENTER, T. H., 1982: Variations in tropical sea surface temperature and surface wind fields associated with the Southern Oscillation/El Niño. *Monthly Weather Review*, **110**, 354–384.

ROZANSKI, K. S., JOHNSEN, S., SCHOTTERER, U., and THOMPSON, L. G., 1997: Reconstruction of past climates from stable isotope records of palaeo-precipitation preserved in continental archives. *Hydrological Sciences–Journal des Sciences Hydrologiques*, **42**, 725–745.

SERVAIN, J., 1991: Simple climatic indices for the tropical Atlantic Ocean and some applications. *Journal of Geophysical Research*, **96**, 15,137–15,146.

SERVAIN, J. and LEGLER, D. M., 1986: Empirical orthogonal function analysis of tropical Atlantic sea surface temperature and wind stress: 1964–1979. *Journal of Geophysical Research*, **91**, 14,181–14,191.

SIROCKO, F., SARNTHEIN, M., ERLENKEUSER, H., LANGE, H., ARNOLD, M., and DUPLESSY, J. C., 1993: Century-scale events in monsoonal climate over the past 24,000 years. *Nature*, **364**, 322–324.

SYNAL, H.-A., BEER, J., SCHOTTERER, U., SUTER, M., and THOMPSON, L. G., 1997: Bomb-produced ^{36}Cl in ice core samples from mountain glaciers. *Glaciers from the Alps: Climate and Environmental Archives, Proceedings*, Paul Scherrer Institut, Villigen, Switzerland, 99–102.

THOMPSON, L. G., 1973: Analysis of the concentration of microparticles in an ice core from Byrd Station, Antarctica. *Ohio State University, Institute of Polar Studies, Report No. 46*, 43 pp.

THOMPSON, L. G. and DANSGAARD, W., 1975. Oxygen isotope and microparticle studies of snow samples from Quelccaya Ice Cap, Peru. *Antarctic Journal of the U.S.*, **10**, 24–26.

THOMPSON, L. G., DAVIS, M. E., MOSLEY-THOMPSON, E., SOWERS, T. A., HENDERSON, K. A., ZAGORODNOV, V. S., LIN, P.-N., MIKHALENKO, V. N., CAMPERN, R. K., BOLZAN, J. F., and COLE-DAI, J., 1998: A 25,000 year tropical climate history from Bolivian ice cores. *Science*, **282**, 1858–1864.

THOMPSON, L. G., MOSLEY-THOMPSON, E., DANSGAARD, W., and GROOTES, P. M., 1986: The "Little Ice Age" as recorded in the stratigraphy of the tropical Quelccaya ice cap. *Science*, **234**, 361–364.

THOMPSON, L. G., MOSLEY-THOMPSON, E., DAVIS, M. E., BOLZAN, J., DAI, J., GUNDESTRUP, N., YAO, T., WU, X., and XIE, Z., 1989: Holocene–Late Wisconsin Pleistocene climatic ice core records from Qinghai-Tibetan Plateau. *Science*, **246**, 474–477.

THOMPSON, L. G., MOSLEY-THOMPSON, E., DAVIS, M. E., LIN, P.-N, HENDERSON, K. A., COLE-DAI, J., BOLZAN, J. F., and LIU, K.-B., 1995: Late glacial stage and Holocene tropical ice core records from Huascarán, Peru. *Science*, **269**, 46–50.

THOMPSON, L. G., MOSLEY-THOMPSON, E., and THOMPSON, P. A., 1992: Reconstructing interannual climate variability from tropical and subtropical ice-core records: *In* Diaz, H. F. and Markgraf, V. (eds.), *El Niño: Paleoclimatic Aspects of the Southern Oscillation*. Cambridge: Cambridge University Press, 295–322.

THOMPSON, L. G., MOSLEY-THOMPSON, E., and MORALES ARNAO, B., 1984: Major El Niño/Southern Oscillation events recorded in stratigraphy of the tropical Quelccaya Ice Cap. *Science*, **226**, 50–52.

THOMPSON, L. G., YAO, T., DAVIS, M. E., HENDERSON, K. A., MOSLEY-THOMPSON, E., LIN, P.-N., BEER, J., SYNAL, H.-A., COLE-DAI, J., and BOLZAN, J. F., 1997: Tropical climate instability: The last glacial cycle from a Qinghai-Tibetan ice core. *Science*, **276**, 1821–1825.

TRENBERTH, K. E., BRANSTATOR, G. W., KAROLY, D., DUMAR, A., LAU, N.-C., and ROPELEWSKI, C., 1998: Progress during TOGA in understanding and modeling global teleconnections associated with tropical sea surface temperatures. *Journal of Geophysical Research*, **103**, 14,291–14,324.

VERNEKAR, A. D., ZHOU, J., and SHUKLA, J., 1995: The effect of the Eurasian snow cover on the Indian monsoon. *Journal of Climate*, **8**, 248–266.

WALLACE. J. M, RASMUSSON, E. M., MITCHELL, T. P., KOUSKY, V. E., SARACHIK, E. S., and van STROCH, H., 1998: On the structure and evolution of ENSO-related climate variablility in the tropical Pacific: Lessons from TOGA. *Journal of Geophysical Research*, **103**, 14,242–24,259.

WEARE, B. C., 1977: Empirical orthogonal function analysis of Atlantic surface temperatures. *Quarterly Journal of the Royal Meterorological Society*, **193**, 467–478.

WEBSTER, P. J., 1983: The large-scale structure of the tropical atmosphere. *In* Hoskins, B. J. and Pierce, R. (eds.), *Large-Scale Dynamic Processes in the Atmosphere*. New York: Academic Press, 235–276.

WEBSTER, P. J., MAGAÑA, V. O., PALMER, T. N., SHUKLA, J., TOMAS, R. A., YANAI, M., and YASUNARI, T., 1998: Monsoons: Process, predictability, and the prospects for prediction. *Journal of Geophysical Research*, **103**, 14,451–14,510.

YASUNARI, T., KITOH, A., and TOKIOKA, T., 1991: Local and remote responses to excessive snow mass over Eurasia appearing in the northern spring and summer climate – A study with the MRI-GCM. *Journal of the Meteorological Society of Japan*, **69**, 473–487.